Compact Modeling of Nonideal Trapping/Detrapping Processes in GaN Power Devices

N. Modolo, *Graduate Student Member, IEEE*, C. De Santi, *Member, IEEE*, G. Baratella, A. Bettini, *Graduate Student Member, IEEE*, M. Borga, N. Posthuma, B. Bakeroot, S. You, S. Decoutere, A. Bevilacqua, *Senior Member, IEEE*, A. Neviani, G. Meneghesso, *Fellow, IEEE*, E. Zanoni, *Life Fellow, IEEE*, and M. Meneghini, *Senior Member, IEEE*

***Abstract*— Compact modeling of charge trapping processes in GaN transistors is of fundamental importance for advanced circuit design. The goal of this article is to propose a methodology for modeling the dynamic characteristics of GaN power HEMTs in the realistic case where trapping/detrapping kinetics are described by stretched exponentials, contrary to ideal pure exponentials, thus significantly improving the state of the art. The analysis is based on: 1) an accurate methodology for describing stretched-exponential transients and extracting the related parameters and 2) a novel compact modeling approach, where the stretched exponential behavior is reproduced via multiple *RC* networks, whose parameters are specifically tuned based on the results of 1). The developed compact model is then used to simulate the transient performance of the HEMT devices as a function of duty cycle and frequency, thus providing insight on the impact of traps during the realistic switching operation.**

***Index Terms*— Activation energy distribution, p-GaN HEMTs, stretched exponential, surface traps, time constant profile extraction, trap-state mapping.**

I. Introduction

GaN-BASED transistors have recently emerged as excellent candidates for next-generation power converters [1]; due to monolithic integration, they are expected to rapidly find application in GaN-based integrated circuits (IC) [2]–[4].

For the design of GaN ICs, accurate compact models are necessary; this need has led to the development of highly sophisticated, physics-based transistors models, such as the advanced SPICE model (ASM) for HEMTs [5], [6] or the Massachusetts Institute of Technology (MIT) virtual source GaN high-voltage (MSVG-HV) model [7].

In several cases, existing models can reproduce very effectively the dc properties of the transistors; however, attention is needed in the presence of charge-trapping phenomena, which may modify the dynamic response of the transistors. Specifically, the presence of single or extended defects may cause charge trapping effects [8], [9], which results in degradation of the switching characteristics, favoring a dynamic-R_{ON} and V_{TH} shift [10]–[14].

Such trapping phenomena need to be analyzed and modeled: state-of-the-art approaches [15]–[17] reproduce trapping/detrapping phenomena as pure exponentials, an approximation that is only valid for ideal point defects, with a single energy level; following this idea, Kellogg *et al.* [16] proposed a method to model defects in GaN HEMTs making use of a three-pole *RC* circuit. However, pure exponentials are generally not representative of real trapping kinetics [18]. In the presence of multiple traps, Li *et al.* [17] suggested an iterative algorithm to extract multiple *RC* units with minimized error. Nonetheless, this extraction lacks physical insight and is not able to predict the temperature dependence of the fit trend, which is of extreme importance.

More recently, Weiser *et al.* [19] proposed a finer approach to model distributed traps by defining a multiple *RC* circuit whose time constant distribution follows a Gaussian shape. However, the Gaussian distribution extraction relies in the (unrealistic) approximation that the kinetic of each single component is a step function instead of an exponential decay. In addition to this, the proposed methodology does not account for temperature dependence.

In the most general formulation (particularly relevant for surface and extended defects), trapping/detrapping transients from point, extended or surface defects can be modeled by a stretched exponential function. The stretched exponential transient can be reproduced as the sum of n ideal

Manuscript received 22 February 2022; revised 12 May 2022; accepted 6 June 2022. Date of publication 30 June 2022; date of current version 25 July 2022. This work was supported in part by the iRel40 Project. iRel40 is a European Co-Funded Innovation Project that has been granted by the Electronics Components and Systems for European Leadership (ECSEL) Joint Undertaking (JU) under Grant 876659. The review of this article was arranged by Editor S. Chowdhury. *(Corresponding author: N. Modolo.)*

N. Modolo, C. De Santi, A. Bettini, A. Bevilacqua, A. Neviani, G. Meneghesso, E. Zanoni, and M. Meneghini are with the Department of Information Engineering, Università degli Studi di Padova, Padua 35131, Italy (e-mail: nicola.modolo@phd.unipd.it; carlo.desanti@unipd.it; andrea.bettini@phd.unipd.it; andrea.bevilacqua@dei.unipd.it; neviani@dei.unipd.it; gauss@dei.unipd.it; zanoni@dei.unipd.it; matteo.meneghini@unipd.it).

G. Baratella and B. Bakeroot are with the CMST, IMEC, Ghent University, B9052 Ghent, Belgium (e-mail: giulio.baratella@imec.be; benoit.bakeroot@imec.be).

M. Borga, N. Posthuma, S. You, and S. Decoutere are with IMEC VZW, B3001 Leuven, Belgium (e-mail: matteo.borga@imec.be; niels.posthuma@imec.be; shuzhen.you@imec.be; stefaan.decoutere@imec.be).

Color versions of one or more figures in this article are available at https://doi.org/10.1109/TED.2022.3184622.

Digital Object Identifier 10.1109/TED.2022.3184622

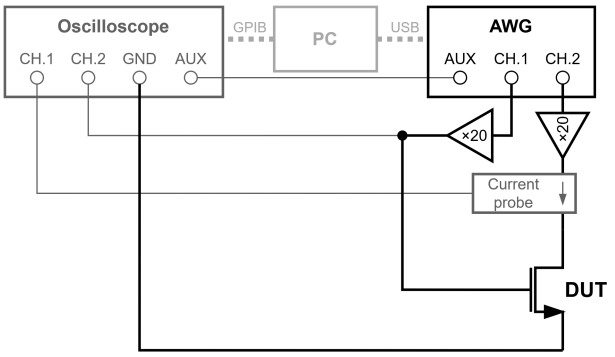

Fig. 1. Simplified schematic of the experimental setup for V_{TH} transient DLTS measurements.

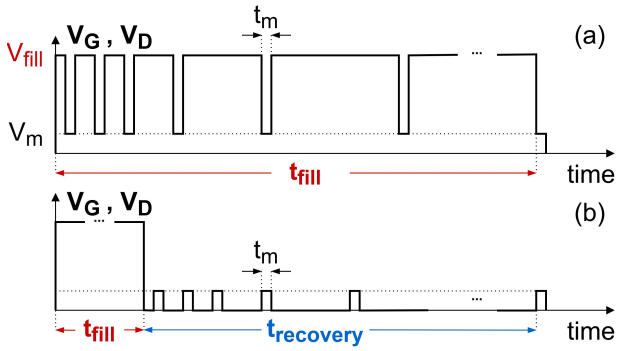

Fig. 2. Waveforms of the logarithmically spaced pulses (V_m) to monitor (a) stress phase and (b) recovery phase.

exponentials [20], [21] as described in the following equation:

$$f(t) = A \cdot \exp\left(-\left(\frac{t}{\tau_0}\right)^{\beta}\right) \approx \sum_{i=1}^{n} A_i \cdot \exp\left(-\frac{t}{\tau_i}\right) \quad (1)$$

where A_i and τ_i are the amplitude and time constants of each process, respectively. Within this article, an original two-step procedure for compact modeling of the dynamic properties of GaN HEMTs is proposed. The methodology is based on: 1) the extraction of the physical properties of the trap through mathematical investigation of the trapping/detrapping kinetics and 2) the implementation via equivalent multiple-*RC* circuit distribution, using Verilog-A in the commercial circuit simulator advanced design systems (ADS) from Agilent [5].

Simulations and experimental data are compared to verify the developed model. Finally, the behavior of the devices is simulated as a function of frequency and duty cycle to provide information on the effect of traps on device performance in realistic switching conditions.

II. Experimental Details and Results

The devices under test are on-wafer E-mode p-GaN HEMTs. Trapping/detrapping experiments were carried out by a custom V_{TH} transient setup [22], schematically represented in Fig. 1. V_{TH} of the device under test (DUT) is monitored both during the filling and recovery phase (see Fig. 2) from the microseconds to the hundreds of seconds.

The DUT is stressed by applying $(V_{Gfill},\ V_{Dfill}) = (0, 10)$ V at different temperatures (30, 90, 150) °C. Fig. 3 shows the V_{TH} shift induced on the device during the filling and recovery

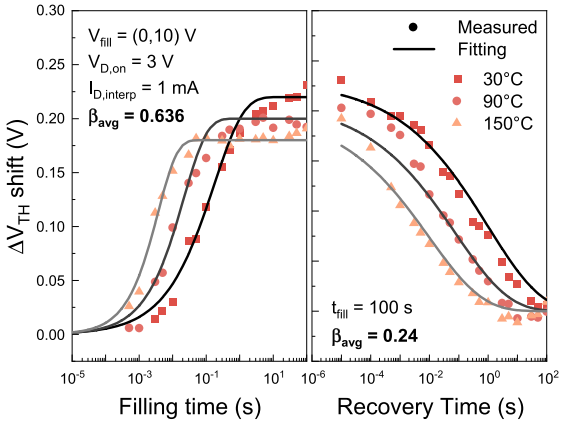

Fig. 3. ΔV_{TH} shift on the DUT when $(V_{Gfill}, V_{Dfill}) = (0,\ 10)$ V is applied. Both the stress and recovery phase are shown. $\beta < 1$ is found, indicative of stretched exponential kinetics.

phase. In both cases, the V_{TH} shift cannot be fit with a pure exponential decay, but with a stretched exponential trend: this indicates that the traps responsible are not localized on a single, discrete level (or at a single position), but have a distribution of time constants that, once superimposed, generate the stretched exponential curve. This behavior is typical for the most common surface, buffer, and interface trapping mechanisms in GaN HEMTs, as recently highlighted in [23] and [24], and confirms the importance of this study.

III. Trap Properties Extraction

The full discussion of the methodology used in this article to extract the time constant distribution of the deep levels of interest can be found in [25]. Here, we provide a brief summary; considering (1), A_i and τ_i are the parameters of the single exponential components constituting the multiexponential threshold voltage transient. In the presence of a continuous distribution of time constants, the threshold voltage shift can be expressed as

$$\Delta V_{TH}(t) = \int_0^{\infty} g(\nu) \cdot \exp(-t\nu) d\nu \quad (2)$$

where $\nu = 1/\tau$ and $g(\nu)$ is the probability density function of the distribution of time constants. The latter can be numerically calculated through the inverse Laplace transform, i.e., by a mathematical transformation carried out directly on the ΔV_{TH} data.

Fig. 4 shows the contour map of the time constant distribution (decay rate probability density function [26]) at different temperatures extracted from the experimentally measured V_{TH} recovery transients in Fig. 3 following the procedure presented in [25]. It is important to stress that the extracted time constant distribution of $f(t)$ does not have a Gaussian shape and differs from the simple derivative of the transient $\mathrm{d}f(t)/d\log(t)$ [27], which has no direct meaning in relation to trap properties.

Once $g(\nu)$ is defined, the trap signature distribution can be extracted from the temperature-dependent time constant distribution. As explained in [25], given a temperature-dependent time constant distribution $(\tau_{i,j},\ A_{i,j},\ T_j)$, from a set of temperature-dependent measurements, such as the one mapped

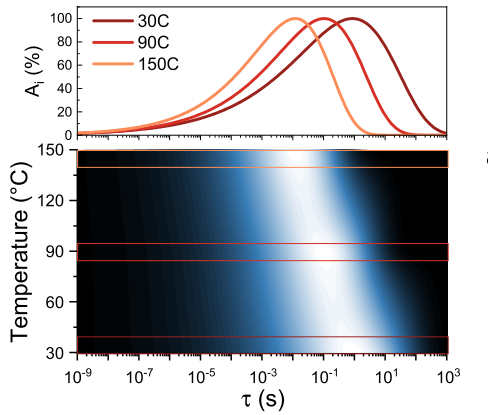

Fig. 4. (Bottom) contour map of the mathematically extracted time constant distribution at different temperatures along with (top) the plot of the spectral amplitude of the trap level at (30, 90, 150) °C.

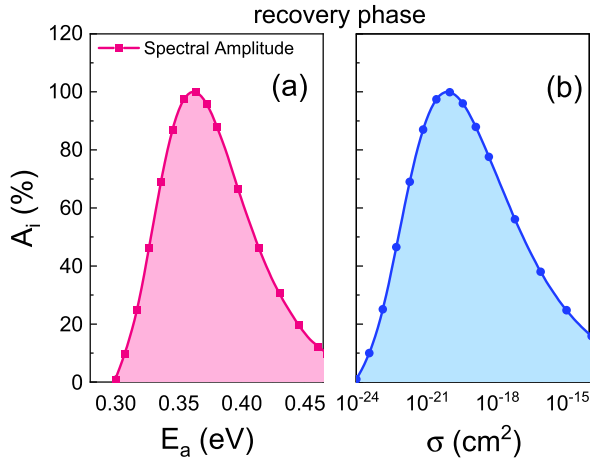

Fig. 5. (a) Distribution of activation energies. (b) Capture cross sections in the DUT, as extracted from temperature-dependent measurements.

in Fig. 4, a distribution of activation energies ($E_{a,i}$) and cross sections ($\sigma_{c,i}$) can be uniquely extracted.

In other words, at a given temperature T_j, a distribution of time constants $\tau_{i,j}$ and amplitudes $A_{i,j}$ can be extracted. By repeating the measurements at several temperatures, the corresponding trap properties can be extrapolated, in terms of activation energy $E_{a,i}$ and cross sections $\sigma_{c,i}$.

Fig. 5 shows the results of this analysis for the recovery phase, where the spectral amplitude of each (E_a, σ_c) component is defined by its relative coefficient A_i. Remarkably, the (E_a, σ_c, A_i) distribution contains all the information on the temperature-dependent characteristics of the trap, which is used in the next section to define the optimal RC distribution to be implemented in a compact model.

In this case, $n = 15$ is used to reproduce the experimental data with excellent accuracy without adversely affecting the computational speed. Lower n values, down to 5, can still provide a good model quality. As theoretically expected, $\sum_{i=1}^{15} A_i = A$, according to the notation in (1).

IV. Compact Model Implementation

The second step of our analysis is the implementation of the (E_a, σ_c, A_i) distribution into a compact model. The most natural way to reproduce an exponential decay function using

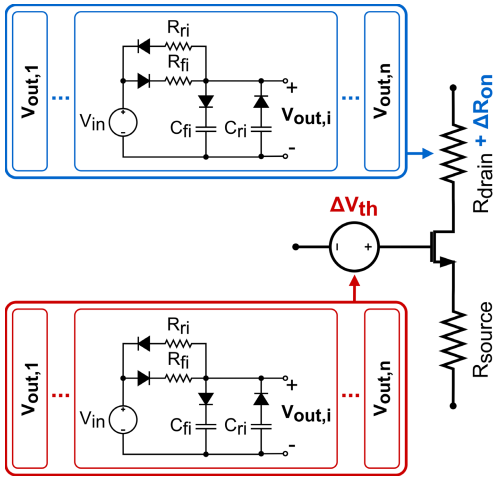

Fig. 6. Schematic representation of how the *n-RC* network extracted from the experimental data is implemented to account for both the dynamic ON-resistance and ΔV_{TH} shift.

electronic passive components is to use an RC network

$$V_{trap}(t) = (\theta_1 V_{DG} + \theta_2(1 - \exp(-\theta_3 V_{DG}))) \cdot R_{trap}\left(1 - \exp\left(-\frac{t}{R_{trap}C_{trap}}\right)\right) \quad (3)$$

where R_{trap} and C_{trap} are related to the capture/emission time constant of the process, respectively, and θ_1, θ_2, and θ_3 are tuning parameters to adjust the contribution of the input stress bias (in this article V_{DG}).

In case of extended defects, a multiple-RC network can be used to implement the time constant distributions into an equivalent circuit having the applied bias as input and the multiexponential time response $\sum V_{trap,i}(t)$ as output; the output of this circuit is then used to calculate the time-dependent variation of R_{ON} and V_{TH} (see Fig. 6).

While the R_i and C_i parameters are meaningful to define the RC circuit, they do not describe the physical characteristics of a trap. Therefore, even if they emulate the time constants of the process at a specific temperature, they are not able to describe how such process is influenced by a change in the temperature. This factor should be considered since phenomena such as self-heating can dynamically change the device temperature.

Consistently with the Arrhenius law [28], each component of the multiple-RC circuit is defined as

$$R_i C_i(T) = \tau_i(T) = \frac{1}{T^2}\exp\left(\frac{E_{a,i}}{kT} + \ln\left(\frac{h^3}{2\sqrt{3}(2\pi)^{\frac{3}{2}} m_r m_0 k^2 g \sigma_{c,i}}\right)\right) \quad (4)$$

where T is the temperature, h is the Planck constant, k is Boltzmann's constant, m_0 and m_r are the rest and effective mass of electrons, respectively, and g is a degeneration factor (typically 1). The spectral amplitude A_i of each exponential component represents its relative weight. This proportional term is assigned to the resistance of the RC network $R_i = A_i$, while $C_i = \tau_i / R_i$.

A variation in temperature, due to self-heating or external stimulus, will impact the time constant of the model in agreement with the experimental data. To consider the

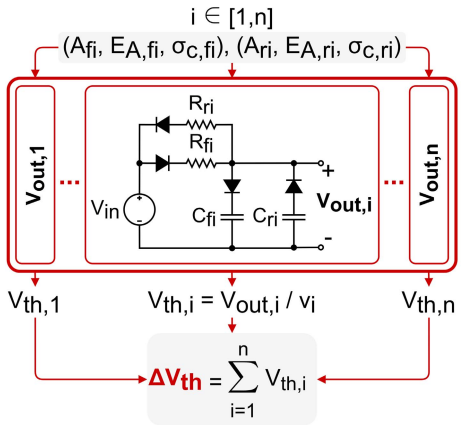

Fig. 7. Two triplets (E_a, σ_c, A_i) reported in Fig. 5 are used as input parameters to build the optimal *RC* network. The *n*-outputs of the module are used to introduce the dynamic ΔV_{TH} shift. In this work, $n = 15$ is used.

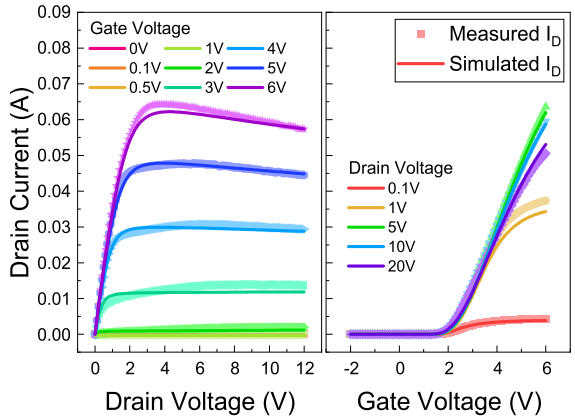

Fig. 8. Compact model is tuned with the dc characteristics of the device. Realistic physical parameters are used. The model accurately reproduces the experimental data.

different behavior during the filling and recovery phase, two (E_a, σ_c, A_i) distributions were extracted from the experimental data and implemented: one for the filling and one for the recovery. This is schematically represented in Fig. 7, which also shows how the input parameters are used to reproduce the overall V_{TH} shift. The developed module is implemented in the ASM GaN model [5], which has been modified to include a p-GaN layer in the gate-stack [29]. The Verilog-A model is then simulated using the built-in Verilog-A compiler of the SPICE-based ADS software.

First, the model parameters are tuned to reproduce the dc characteristic of the DUT with excellent accuracy (see Fig. 8). Then, the (E_a, σ_c, A_i) distributions in filling and recovery conditions extracted from the experimental V_{TH} transient measurements are added to the trap model. Fig. 9 summarizes the comparison between the transient simulation and the experimental data together with the applied simulation waveforms. An excellent agreement in reproducing the time-dependent V_{TH} shift when (V_{Gfill}, V_{Dfill}) = (0, 10) V is obtained.

The simulation quality with the same set of parameters is equally good at different temperatures, demonstrating that the developed model can emulate the dynamic response of the device in a wide temperature range. The model was tested under different bias conditions, and the results show consistent behavior and accuracy. For sake of simplicity, here, we focus only on the (V_{Gfill}, V_{Dfill}) = (0, 10) V condition.

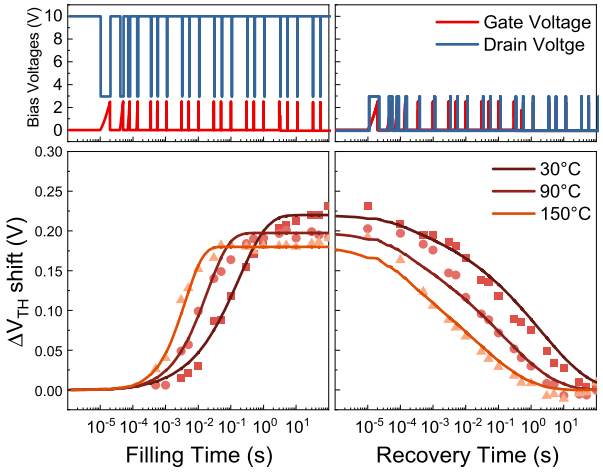

Fig. 9. Comparison between the transient simulation obtained via compact modeling and experimental data along with the applied bias. The simulation shows excellent accuracy in reproducing the dynamic behavior of the DUT, also as a function of temperature.

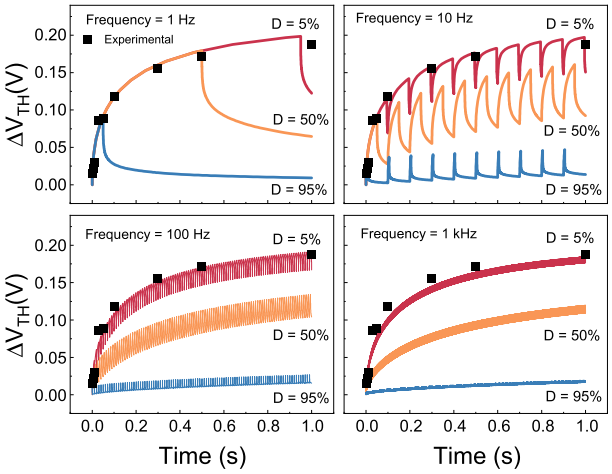

Fig. 10. Matrix of simulations showing both the effect of duty cycle and frequency in the dynamic response of the device. The frequency defines the amplitude of the trapping/detrapping kinetics, whereas the duty cycle defines the trajectory of the cumulative shift. Comparison with experimental data is shown, demonstrating excellent agreement.

V. Operating Frequency and Duty Cycle

A self-consistent and physics-based compact model can give insight on the interplay between the capture and emission processes in various operating conditions. Such aspects are particularly relevant in the circuit design. Fig. 10 shows the time-domain simulation when the device is biased for 1 s at different duty cycles and frequencies.

The result shows that in the present case, since the recovery spectrum has shorter time constants than the filling spectrum, the higher the frequency, the smaller the amplitude of the overall capture plus emission process per cycle. On the other hand, the ΔV_{TH} trajectory and saturation values are defined by the t_{ON}/t_{OFF} ratio (duty cycle) since this parameter defines the balance between the filling and the recovery time constants. Fig. 11 summarizes the ΔV_{TH} shift versus the applied frequency after a certain number of cycles.

Three regions can be distinguished.

1) $f < 1$ *Hz:* The number of cycles has no effect since the trapping is complete at each cycle and no cumulative trapping is present. When the frequency increases, the overall ΔV_{TH}

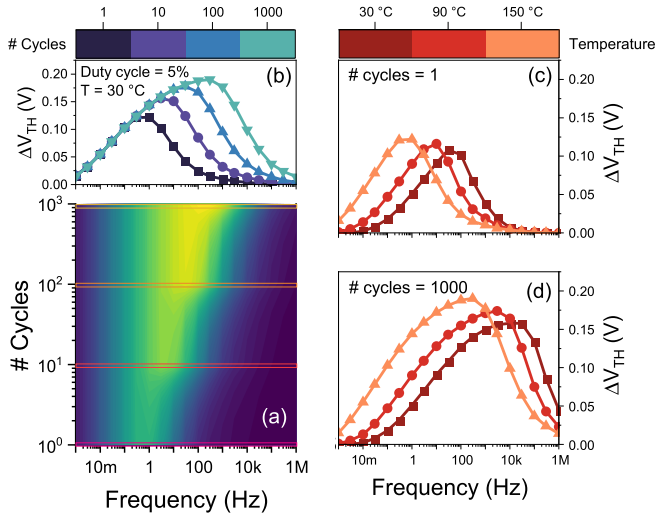

Fig. 11. Novel benchmark for GaN HEMT performance. (a) and (b) Map (which indicates in false color the total V_{TH} shift for a given frequency and number of duty cycles) can be used to assess the dynamic degradation of the main device parameters, i.e., ($\Delta V_{TH} - \Delta R_{ON}$), in real operating conditions. (c) and (d) Higher the temperature, the faster the cumulative effect.

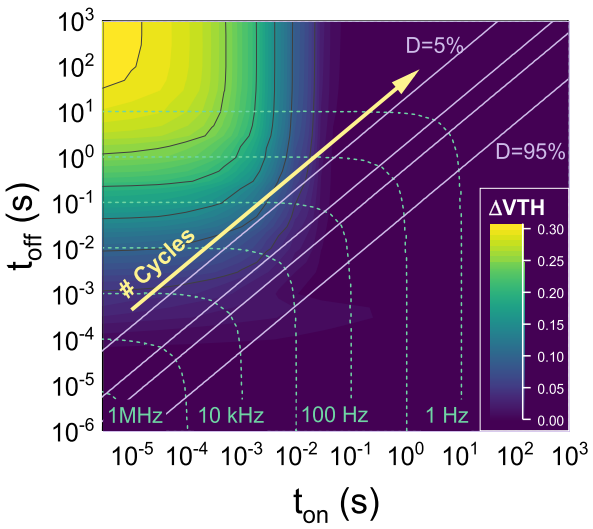

Fig. 12. Contour map of the ΔV_{TH} shift together with the iso-frequency and iso-duty-cycle loci. The lower the duty cycle and the lower the frequency, the closer the trajectory of the cumulative effect to the critical ΔV_{TH} region.

increases, due to the reduced t_{ON} available for the recovery. At the lowest frequencies, t_{ON} is long enough to completely recover, and no threshold voltage shift is visible.

2) $1 < f < 10^4$ *kHz:* The filling time is not sufficient to fill all traps; therefore, cumulative trapping is present and the overall ΔV_{TH} is higher for a larger number of trapping cycles. When the frequency increases, a peak in ΔV_{TH} is visible. This corresponds to the crossing point of the filling time constant distribution: after the peak, the trapping time t_{OFF} is short enough to cause a lower level of trapping and ΔV_{TH} decreases. The peak is located at a frequency value higher for a higher number of cycles since the cumulative trapping is still present.

3) $f > 10^4$ *kHz:* The trapping time t_{OFF} is too short compared to the time constants in the filling spectrum, and therefore, the amount of trapping becomes negligible and ΔV_{TH} approaches 0. The cumulative trapping is still present, so a higher number of cycles cause some level of V_{TH} shift, but eventually, they will cause no ΔV_{TH} for high enough frequency. The simulation result confirms that at higher temperature, the capture/emission ratio may change, thus changing the worst case condition, as shown in Fig. 11(c) and (d). It is important to point out that the overall shape and behavior depends on the balance between the time constants in the filling and in the recovery spectrum; therefore, it will change in devices with different distribution widths and center time constant values.

The results in Figs. 10 and 11 predict that the cumulative effect resulting from the t_{ON}/t_{OFF} ratio will take place even in the megahertz range; nevertheless, this region appears to be a relatively safe region compared to the results in Fig. 3, if the device is operated long enough. Finally, the V_{TH} transient has been repeated for increasing filling times, from 1 μs to 1000 s at (V_{Gfill}, V_{Dfill}) = (0, 10). A surface map, in which each value of the matrix represents ΔV_{TH} after a certain fill time (t_{OFF}) and recovery time (t_{ON}), was built.

Fig. 12 shows the contour map of the V_{TH} shift together with the iso-frequency and iso-duty-cycle loci. These results highlight how, in circuit design, the choice of frequency and duty cycle draws a trajectory that impacts on the instability of a device, which depends on the balance between trap filling/discharging times.

Furthermore, in accordance with Figs. 10 and 11, the trajectory of the instability will be reached at any frequency when a sufficiently high number of cycles will be completed. These results are extremely important because they give an insight on the criticality of a trap depending on its capture and emission time maps.

Indeed, some traps that can be detected in high concentration by common experimental techniques, and that cause significant dynamic performance worsening, may never appear in real operating conditions, depending on the experimental parameters and timings used for detection.

The results in Figs. 10 and 11 are obtained from the experimentally tuned and physically tuned compact model and summarize all the possible operating conditions of the DUT. Due to the developed analysis and model, it is possible to accurately predict the behavior of the device in a wide range of operating conditions, starting from the analysis of single trapping/detrapping kinetics.

VI. Conclusion

In this article, a new approach for compact modeling of the stretched exponential trapping/detrapping kinetics of GaN HEMTs is proposed. First, physically meaningful trap parameters are extracted based on mathematical processing of the experimental data, as a function of temperature. Second, the trap signature is implemented in a p-GaN HEMT compact model, making use of two multiple-*RC* networks, one for trapping and one for detrapping. The SPICE-based simulations show excellent agreement with the experimental data obtained by means of V_{TH} transients.

The physics-based trap model is then used to gain insight on the dynamic behavior of the devices as a function of the operating frequency and duty cycle. Novel insight on the GaN HEMT dynamic performance degradation is given highlighting

how the criticality of a trap is dependent on its location in the capture and emission time map. The duty cycle plays a key role in determining the performance degradation trajectory, while the frequency is related to the amplitude of the capture and emission process per cycle.

The proposed approach is of paramount importance for circuit designers, who need to accurately reproduce the trapping/detrapping phenomena in various operating conditions, and for the detection of the dynamic performance worsening by common experimental techniques, which may overestimate or underestimate the real behavior depending on the specific experimental conditions and timings they employ.

ACKNOWLEDGMENT

This activity was supported by project iRel40. iRel40 is a European co-funded innovation project that has been granted by the ECSEL Joint Undertaking (JU) under Grant Agreement No. 876659. The funding of the project comes from the Horizon 2020 research program and participating countries. National funding is provided by Germany, including the Free States of Saxony and Thuringia, Austria, Belgium, Finland, France, Italy, The Netherlands, Slovakia, Spain, Sweden, and Turkey. This project is co-funded by the Ministry of Economic Development in Italy.

REFERENCES

[1] H. Amano *et al.*, "The 2018 GaN power electronics roadmap," *J. Phys. D, Appl. Phys.*, vol. 51, no. 16, 2018, Art. no. 163001.

[2] X. Li *et al.*, "Integration of 650 V GaN power ICs on 200 mm engineered substrates," *IEEE Trans. Semicond. Manuf.*, vol. 33, no. 4, pp. 534–538, Nov. 2020, doi: 10.1109/TSM.2020.3017703.

[3] X. Li *et al.*, "GaN-on-SOI: Monolithically integrated all-GaN ICs for power conversion," in *IEDM Tech. Dig.*, 2019, pp. 4.4.1–4.4.4, doi: 10.1109/IEDM19573.2019.8993572.

[4] H. Wang, A. M. H. Kwan, Q. Jiang, and K. J. Chen, "A GaN pulse width modulation integrated circuit for GaN power converters," *IEEE Trans. Electron Devices*, vol. 62, no. 4, pp. 1143–1149, Apr. 2015, doi: 10.1109/TED.2015.2396649.

[5] S. Khandelwal *et al.*, "ASM GaN: Industry standard model for GaN RF and power devices—Part 1: DC, CV, and RF model," *IEEE Trans. Electron Devices*, vol. 66, no. 1, pp. 80–86, Jan. 2019, doi: 10.1109/TED.2018.2867874.

[6] S. Khandelwal and T. A. Fjeldly, "A physics based compact model of I–V and C–V characteristics in AlGaN/GaN HEMT devices," *Solid-State Electron.*, vol. 76, pp. 60–66, Oct. 2012, doi: 10.1016/j.sse.2012.05.054.

[7] U. Radhakrishna, T. Imada, T. Palacios, and D. Antoniadis, "MIT virtual source GaNFET-high voltage (MVSG-HV) model: A physics based compact model for HV-GaN HEMTs," *Phys. Status Solidi C*, vol. 11, nos. 3–4, pp. 848–852, Mar. 2014, doi: 10.1002/PSSC.201300392.

[8] M. Meneghini *et al.*, "Trapping and reliability assessment in D-mode GaN-based MIS-HEMTs for power applications," *IEEE Trans. Power Electron.*, vol. 29, no. 5, pp. 2199–2207, May 2014, doi: 10.1109/TPEL.2013.2271977.

[9] M. Meneghini *et al.*, "Time- and field-dependent trapping in GaN-based enhancement-mode transistors with p-gate," *IEEE Electron Device Lett.*, vol. 33, no. 3, pp. 375–377, Mar. 2012, doi: 10.1109/LED.2011.2181815.

[10] X. Li *et al.*, "Investigating the current collapse mechanisms of p-GaN gate HEMTs by different passivation dielectrics," *IEEE Trans. Power Electron.*, vol. 36, no. 5, pp. 4927–4930, May 2021, doi: 10.1109/TPEL.2020.3031680.

[11] N. Modolo *et al.*, "Cumulative hot-electron trapping in GaN-based power HEMTs observed by an ultra-fast (10 V/ns) on-wafer methodology," *IEEE J. Emerg. Sel. Topics Power Electron.*, early access, May 3, 2021, doi: 10.1109/JESTPE.2021.3077127.

[12] X. Tang, B. Li, H. A. Moghadam, P. Tanner, J. Han, and S. Dimitrijev, "Mechanism of threshold voltage shift in p-GaN gate AlGaN/GaN transistors," *IEEE Electron Device Lett.*, vol. 39, no. 8, pp. 1145–1148, Aug. 2018, doi: 10.1109/LED.2018.2847669.

[13] S. Tam, P.-K. Ko, and C. Hu, "Lucky-electron model of channel hot-electron injection in MOSFET's," *IEEE Trans. Electron Devices*, vol. ED-31, no. 9, pp. 1116–1125, Sep. 1984, doi: 10.1109/TED.1984.21674.

[14] M. J. Uren and M. Kuball, "Impact of carbon in the buffer on power switching GaN-on-Si and RF GaN-on-SiC HEMTs," *Jpn. J. Appl. Phys.*, vol. 60, no. SB, May 2021, Art. no. SB0802, doi: 10.35848/1347-4065/abdb82.

[15] S. A. Albahrani, D. Mahajan, J. Hodges, Y. S. Chauhan, and S. Khandelwal, "ASM GaN: Industry standard model for GaN RF and power devices—Part-II: Modeling of charge trapping," *IEEE Trans. Electron Devices*, vol. 66, no. 1, pp. 87–94, Jan. 2019, doi: 10.1109/TED.2018.2868261.

[16] K. Kellogg, S. Khandelwal, L. Dunleavy, and J. Wang, "Characterization of thermal and trapping time constants in a GaN HEMT," in *Proc. ARFTG*, 2020, pp. 20–23, doi: 10.1109/ARFTG47584.2020.9071731.

[17] K. Li, P. L. Evans, and C. M. Johnson, "Characterisation and modeling of Gallium nitride power semiconductor devices dynamic on-state resistance," *IEEE Trans. Power Electron.*, vol. 33, no. 6, pp. 5262–5273, Jun. 2018, doi: 10.1109/TPEL.2017.2730260.

[18] N. Modolo *et al.*, "Understanding the effects of off-state and hard-switching stress in gallium nitride-based power transistors," *Semicond. Sci. Technol.*, vol. 36, no. 1, 2020, Art. no. 014001, doi: 10.1088/1361-6641/abc456.

[19] M. C. J. Weiser, J. Huckelheim, and I. Kallfass, "A novel approach for the modeling of the dynamic ON-state resistance of GaN-HEMTs," *IEEE Trans. Electron Devices*, vol. 68, no. 9, pp. 4302–4309, Sep. 2021, doi: 10.1109/TED.2021.3098498.

[20] D. C. Johnston, "Stretched exponential relaxation arising from a continuous sum of exponential decays," *Phys. Rev. B, Condens. Matter*, vol. 74, no. 18, Nov. 2006, Art. no. 184430, doi: 10.1103/PhysRevB.74.184430.

[21] J. Joh and J. A. del Alamo, "A current-transient methodology for trap analysis for GaN high electron mobility transistors," *IEEE Trans. Electron Devices*, vol. 58, no. 1, pp. 132–140, Jan. 2011, doi: 10.1109/TED.2010.2087339.

[22] N. Modolo *et al.*, "A physics-based approach to model hot-electron trapping kinetics in p-GaN HEMTs," *IEEE Electron Device Lett.*, vol. 42, no. 5, pp. 673–676, May 2021, doi: 10.1109/LED.2021.3067796.

[23] A. Minetto *et al.*, "Drain field plate impact on the hard-switching performance of AlGaN/GaN HEMTs," *IEEE Trans. Electron Devices*, vol. 68, no. 10, pp. 5003–5008, Aug. 2021, doi: 10.1109/TED.2021.3101182.

[24] M. Matys, R. Stoklas, J. Kuzmik, B. Adamowicz, Z. Yatabe, and T. Hashizume, "Characterization of capture cross sections of interface states in dielectric/III-nitride heterojunction structures," *J. Appl. Phys.*, vol. 119, no. 20, May 2016, Art. no. 205304, doi: 10.1063/1.4952708.

[25] N. Modolo *et al.*, "Trap-state mapping to model GaN transistors dynamic performance," *Sci. Rep.*, vol. 12, no. 1, pp. 1–10, Feb. 2022, doi: 10.1038/s41598-022-05830-7.

[26] G. Zatryb, A. Podhorodecki, J. Misiewicz, J. Cardin, and F. Gourbilleau, "On the nature of the stretched exponential photoluminescence decay for silicon nanocrystals," *Nanosci. Res. Lett.*, vol. 6, no. 1, pp. 2–9, Dec. 2011, doi: 10.1186/1556-276X-6-106.

[27] D. Bisi *et al.*, "Deep-level characterization in GaN HEMTs—Part I: Advantages and limitations of drain current transient measurements," *IEEE Trans. Electron Devices*, vol. 60, no. 10, pp. 3166–3175, Oct. 2013, doi: 10.1109/TED.2013.2279021.

[28] J. Zhu *et al.*, "Exponential dependence of capture cross section on activation energy for interface traps in Al_2O_3/AlN/AlGaN/GaN metal-insulator-semiconductor heterostructures," *Appl. Phys. Lett.*, vol. 111, no. 16, Oct. 2017, Art. no. 163502, doi: 10.1063/1.4985592.

[29] N. Modolo, S.-W. Tang, H.-J. Jiang, C. De Santi, M. Meneghini, and T.-L. Wu, "A novel physics-based approach to analyze and model E-Mode p-GaN power HEMTs," *IEEE Trans. Electron Devices*, vol. 68, no. 4, pp. 1489–1494, Apr. 2021, doi: 10.1109/TED.2020.2992587.

Open Access funding provided by 'Università degli Studi di Padova' within the CRUI-CARE Agreement